$4 \times 10^{11}$ Mo $K\alpha_1$ photons $s^{-1}$ $m^{-2}$, $C = 0.5$ and $\delta = 30$ μm (Chikawa, 1974) in (7.1.7.3). In order to improve the resolution further, $q$ must be as high as possible even when $\nu_p$ is increased by 10–100 by use of synchrotron radiation, because $R_I$ decreases with improving resolution (decreasing $\delta$). (Note that $C$ is not expected to increase much with improving resolution.) For example, to keep $R_I$ at the same level as the previous case, $q$ should be 0.7, say, for $\nu_p = 10^{13}$ photons $s^{-1}$ $m^{-2}$ and $\delta = 6$ μm. However, resolution and detection efficiency are, in general, mutually exclusive; the resolution of X-ray sensing photoconductive or phosphor materials is determined by the sizes of their grains and their sensitivities decrease with decreasing grain sizes. High resolution, without sacrificing detection efficiency, has been obtained with an amorphous Se–As alloy photoconductive layer, which has the advantage that no degradation of resolution occurs on increasing the layer thickness (Chikawa, Sato, Kawamura, Kuriyama, Yamashita & Goto, 1986). A layer with a thickness of 20 μm has an absorption efficiency of $q = 0.52$ for Mo $K\alpha$. The resolution of these tubes is shown with their modulation transfer functions in Fig. 7.1.7.2. The limiting resolution of 6 μm was obtained by making the scanning electron beam narrower with a diode-type electron gun have a barium-impregnated tungsten cathode (DIS type) (Chikawa, 1999). The Se–As layer shows very low lag characteristics (less than 1% after one frame).

This type of camera tube was developed primarily for TV broadcasting use and named 'Saticon' as the acronym for the components of the photoconductor, Se, As and Te. (Te enhances the sensitivity to red light.)

Such camera tubes have excellent linearity. The output signal current is proportional to the incident X-ray intensity up to 4 μA. The amplifier is always improving in signal-to-noise ratio, and, at present, the noise level of video amplifiers is ~0.2 nA; it is equivalent to an input intensity of $\sim 10^{11}$ Mo $K\alpha$ photons $m^{-2}$ $s^{-1}$ in the US/Japan standard scanning system (30 frames $s^{-1}$).

Therefore, it is important to increase conversion efficiency ($\eta_1, \eta_2, \ldots, \eta_s$). With increasing voltage applied on the photoconductive layer, the signal current is saturated (in Fig. 7.1.7.1, all the holes produced by an incident photon are collected), and then increases again further by avalanche amplification, as shown in Fig. 7.1.7.3; holes accelerated by a strong electric field cause their multiplication (Sato, Maruyama, Goto, Fujimoto, Shidara, Kawamura, Hirai, Sakai & Chikawa, 1993). It was referred to as 'HARP' (high-gain avalanche-rushing amorphous photoconductor). Together with the signal current, the dark current also increases as shown in Fig. 7.1.7.3. By allowing it to increase to the noise level of the video amplifier, an order of magnitude higher SNR can be achieved. Consequently, individual X-ray photons can be imaged as spots with a size resulting from the point-spread function, unless they are absorbed near the back surface of the photoconductive layer. For X-ray detection, a thick HARP layer should be employed with a very high applied voltage, and stable operation with avalanche amplification was confirmed for a 25 μm thick HARP layer. These pilot tubes were fabricated with a conventional electron gun and had a resolution of about 25 μm.

In general, avalanche amplification results in degradation of spatial resolution and has been used for zero-dimensional detection such as solid-state detectors. To make two-dimensional detection, isolation of each picture element is required. For the HARP, however, no appreciable degradation of resolution due to avalanche amplification was confirmed with a DIS-type tube having an 8 μm thick HARP layer by using visible light through a glass window. X-ray sensitive DIS-type tubes are now commercially available.

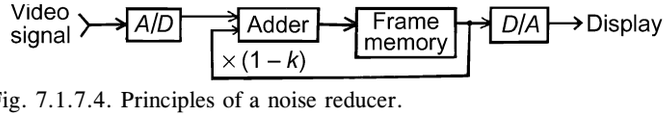


Fig. 7.1.7.4. Principles of a noise reducer.

### 7.1.7.3. *Image processing*

The resolution $\delta$ and integration time $t$ should be selected appropriately according to experimental requirements (Chikawa, 1980). For example, when topographic images of a single dislocation in silicon were observed with $t = 1/30$ s by synchrotron radiation, their contrast and SNR were found to be $C = 0.5$ and $R_I = 20$ for $\delta = 30$ μm, and $C = 1$ and $R_I = 8$ for $\delta = 6$ μm. Since the SNR is desired to be 100, the integration time should be as large as possible unless images of moving objects are degraded. Digital image processing (Heynes, 1977) enables one to adjust the integration time easily. As an example, a noise reducer (McMann, Kreinik, Moore, Kaiser & Rossi, 1978; Rossi, 1978) is shown in Fig. 7.1.7.4. The video signal is sampled and digitized by the $A/D$ converter and the digital video is sent to the adder and thence to the memory. Image information in the memory is continually sent both to the adder through the multiplier for combination with incoming data and to the display through the $D/A$ converter. The weighting of new to old data is made by changing the factor $k$ of the multiplier in the range $0 \leq k \leq 1$. For $k = 0$, the original input image is displayed. In the range $0 < k < 1$, a sliding summation of successive frames is displayed, and the SNR is improved by a factor of $[(1 + k)/(1 - k)]^{1/2}$. The factor $k$ can be adjusted automatically by detecting the difference between successive frames.

Using a HARP tube, the SNR can be improved without integration of the amplifier noise by image processing, and topographs were displayed with an intensity of $\nu_p \simeq 10^9$ photons $s^{-1}$ $m^{-2}$ by a conventional X-ray generator.

Acquisition of extremely low intensity images, dramatic improvements in SNR *via* frame integration, and isolation and enhancement of selected-contrast ranges are possible by digital image processing (Chikawa & Kuriyama, 1991).

## 7.1.8. Storage phosphors (By Y. Amemiya and J. Chikawa)

A storage phosphor, called an 'imaging plate', is a two-dimensional detector having a high detective quantum efficiency (DQE) and a large dynamic range. It was developed in the early 1980's for diagnostic radiography (Sonoda, Takano, Miyahara & Kato, 1983; Kato, Miyahara & Takano, 1985). The performance characteristics of the imaging plate was quantitatively evaluated in the mid 1980's (Miyahara, Takahashi, Amemiya, Kamiya & Satow, 1986) and it was proved to be very useful also for X-ray diffraction experiments (Amemiya, Wakabayashi, Tanaka, Ueno & Miyahara, 1987; Amemiya & Miyahara, 1988). The imaging plate has replaced conventional X-ray film in many X-ray diffraction experiments.

The imaging plate (IP) is a flexible plastic plate that is coated with bunches of very small crystals (grain size about 5 μm) of photo-stimulable phosphor [previously BaFBr:$Eu^{2+}$, recently BaF(Br,I):$Eu^{2+}$] by using an organic binder. The photo-stimulable phosphor is capable of storing a fraction of the absorbed X-ray energy. When later stimulated by visible light, it emits photo-stimulated luminescence (PSL), the intensity of which is proportional to the absorbed X-ray intensity.

The mechanism of PSL is illustrated in Fig. 7.1.8.1. When the IP absorbs incoming X-rays, some of the electrons in the valence band are pumped up to the conduction band of the phosphor crystals. (This corresponds to ionization of $Eu^{2+}$ to $Eu^{3+}$.) The electrons, in turn, are trapped in $Br^-$ and $F^-$ vacancies, which were intentionally introduced in the phosphor crystals during the manufacturing process, forming temporary colour centres, termed *F*-centres. Exposure to visible light again pumps up the trapped electrons so that they generate energy for luminescence, while returning to the valence band of the crystal. (This process corresponds to a recombination of electrons with $Eu^{3+}$ ions, resulting in $Eu^{2+}$ luminescence.) Because the response time of the PSL is as short as 0.8 μs, it is possible to read an X-ray image with a speed of 5–10 μs per pixel with high efficiency. The PSL is based on the allowable transition from $5d$ to $4f$ of $Eu^{2+}$. The wavelength of the PSL ($\lambda \simeq 390$ nm) is reasonably separated from that of the stimulating light ($\lambda = 632.8$ nm), allowing it to be collected by a conventional high-quantum-efficiency photomultiplier tube (PMT). The output of the PMT is amplified and converted to a digital image, which can be processed by a computer. The residual image on the IP can be completely erased by irradiation with visible light, to allow repeated use. The IP is easy to handle, because it is flexible, like a film, and can be kept in light before its exposure to X-rays.

The measured DQE of the IP is shown as a function of the X-ray exposure level together with that of a high-sensitivity X-ray film (Kodak DEF-5) in Fig. 7.1.8.2. The advantage of the IP over X-ray film in DQE is clearly enhanced at lower exposure levels. This arises from the fact that the background noise level of the IP is much smaller than that of X-ray film. The background noise level of the IP corresponds to the signal level of less than 3 X-ray photons/100 μm$^2$. This value compares favourably with the chemical 'fog' level of X-ray film, which amounts to 1000 X-ray photons per equivalent area. The background noise level of the IP depends largely on the performance of the IP read-out system, and it can be smaller than that of a single X-ray photon with a well designed IP read-out system (Amemiya, Matsushita, Nakagawa, Satow, Miyahara & Chikawa, 1988). The DQE of the IP decreases at higher exposure levels owing to 'system fluctuation noise'. Fig. 7.1.8.3 shows the fluctuation noise of the IP and X-ray film as a function of the X-ray exposure level. It is shown that the noise fluctuation at high exposure levels is governed by system fluctuation noise, which amounts to about 1%. Fig. 7.1.8.4 shows the propagation of signal and noise in the IP system. The origins of the system fluctuation noise are non-uniformity of absorption, non-uniformity of the colour-centre density, fluctuation of the laser intensity, non-uniformity of PSL collection, and fluctuation of the high-voltage supply to the PMT. Although it might be possible to reduce the total system fluctuation noise from ~1% to ~0.5%, it is very difficult to reduce it down to <0.1%. This means that the ultimate precision in intensity measurements with the IP is limited to the order of ~0.5%.

Compared to X-ray film, the dynamic range of the IP is much wider, of the order of 1:10$^5$ (Fig. 7.1.8.5). The response of the PSL is linear over the range from 8 to 40 000 photons/(100 μm$^2$), with an error rate of less than 5%. It is shown that the dynamic range of an IP is extended towards the lower exposure levels of X-ray film, but not to the higher exposure levels. The dynamic range of the IP is practically limited to four orders of magnitude by that of the PMT during the read-out. Two sets of PMT's are used in some read-out systems in order to cover the entire dynamic range of the IP.

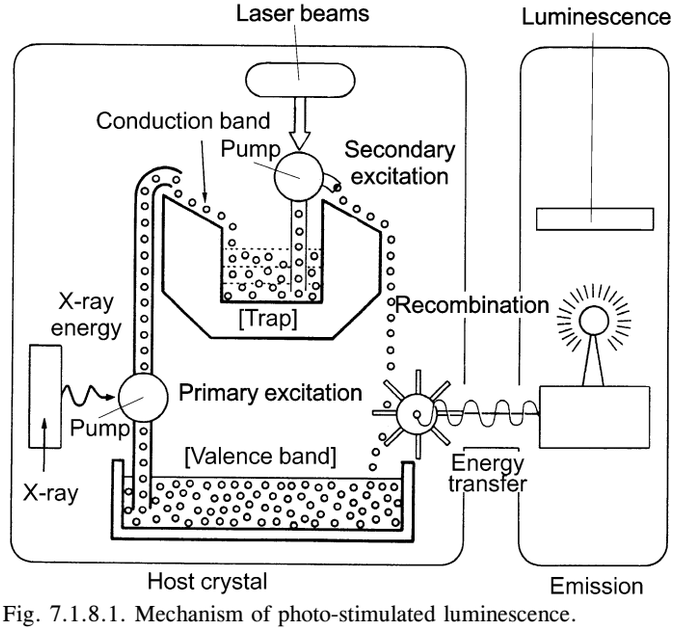


Fig. 7.1.8.1. Mechanism of photo-stimulated luminescence.

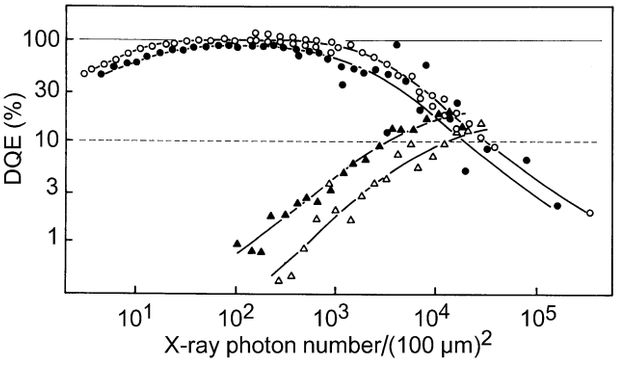


Fig. 7.1.8.2. Measured detective quantum efficiency (DQE) of the imaging plate and high-sensitivity X-ray film as a function of the exposure level. The circles correspond to the imaging plate (with the FCR 101 read-out system, Fuji Film Co. Ltd), triangles to the X-ray film (Kodak DEF-5). The filled symbols are for 8.9 keV and open symbols for 17.4 keV. The solid line indicates a noiseless counter of 100% absorption efficiency (ideal detector). The dashed line indicates a noiseless counter of 10% absorption efficiency (Amemiya & Miyahara, 1988).

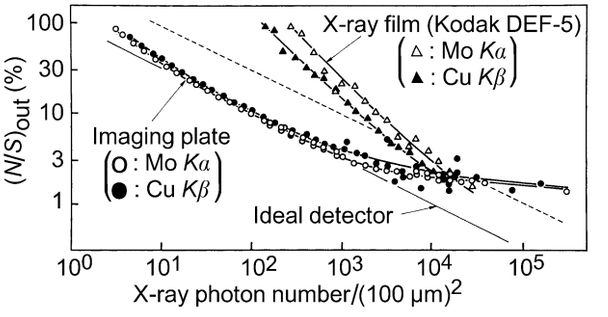


Fig. 7.1.8.3. Fluctuation noise in the signal as a function of the exposure level. The circles correspond to the imaging plate and the triangles to the X-ray film (Kodak DEF-5). The filled symbols are for 8.9 keV and the open symbols for 17.4 keV. The dashed line indicates a noiseless counter of 10% absorption efficiency (Miyahara, Takahashi, Amemiya, Kamiya & Satow, 1986).

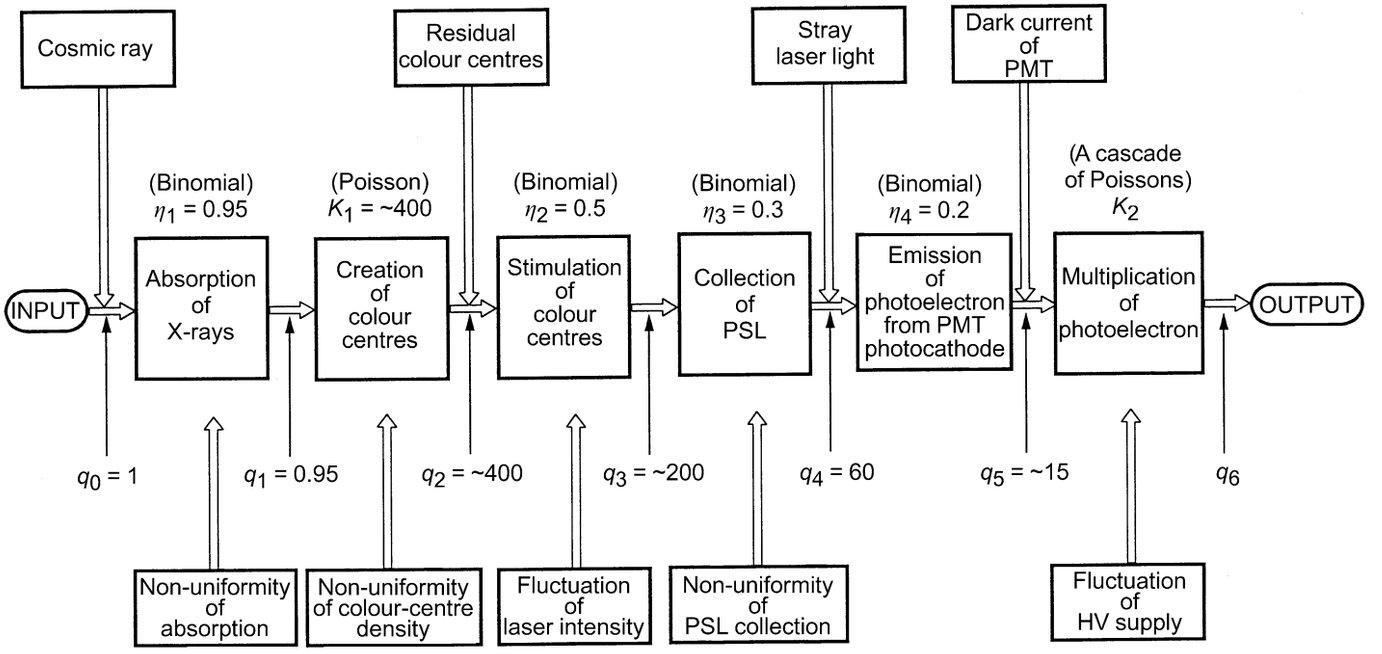


Fig. 7.1.8.4. Diagram showing a cascade of stochastic elementary processes during X-ray exposure and image read out of the imaging plate. The probability distribution of each stochastic process is described in parentheses together with the mean value. The numbers of the quanta, $q_i$ ($i = 0, 5$), are also shown. The noise elements of the upper line contribute to the background noise, which reduces the DQE at lower exposure levels. The noise elements of the bottom line contribute to the system fluctuation noise, which reduces the DQE at higher exposure levels (Amemiya, 1995).

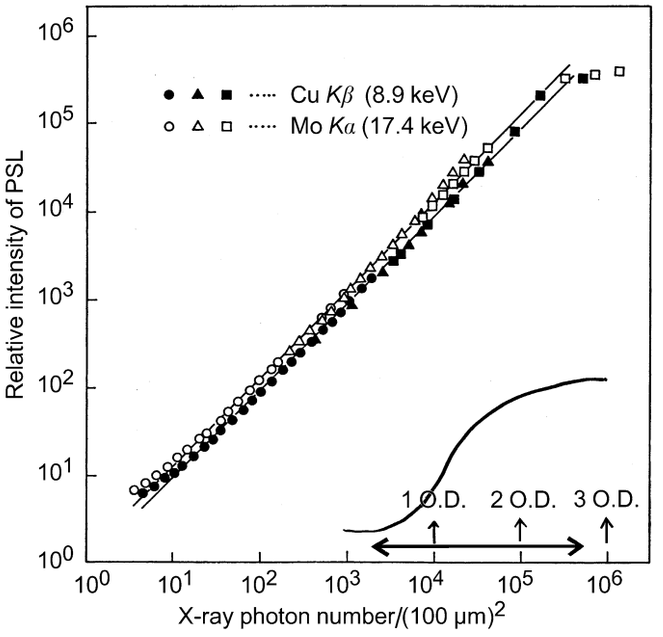


Fig. 7.1.8.5. Dynamic range of the photo-stimulated luminescence of the imaging plate. The dynamic range of typical high-sensitivity X-ray films is also shown. O.D. refers to optical density (Amemiya, 1995).

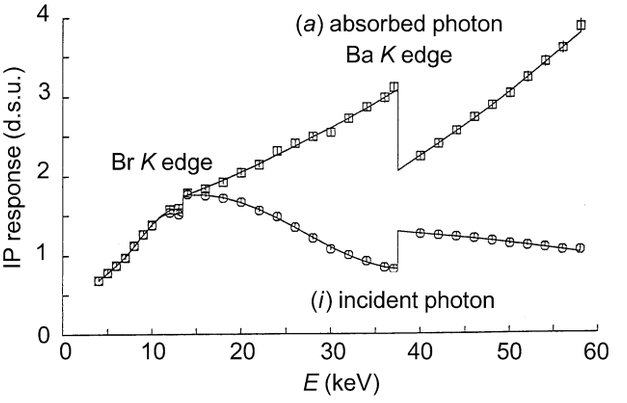


Fig. 7.1.8.6. Dependence of the IP response as a function of the energy of an X-ray photon. (*i*) is the IP response per an incident X-ray photon, and (*a*) the IP response per absorbed X-ray photon. The unit of the ordinate corresponds to the background noise level of the IP scanner (Ito & Amemiya, 1991).

The spatial resolution of the standard IP with a 100 μm laser scanning pitch is 170 μm at the full width at half-maximum (FWHM). The spatial resolution is limited by laser-light scattering in the phosphor during the read-out. A high-resolution IP that includes blue pigments in the phosphor to minimize the laser-light scattering has been developed. A spatial resolution of 43 μm is obtained at a 25 μm laser scanning pitch with the high-resolution IP with the sacrifice of 30% of the amount of PSL. The active area sizes of the available IP range from 127 × 127, 201 × 252, 201 × 400 to 800 × 400 mm.

The IP response per incident X-ray photon is shown as a function of the X-ray energy in Fig. 7.1.8.6, together with the deposited energy per absorbed X-ray photon. The abrupt decrease in the energy deposition above the barium *K*-absorption edge is due to the energy escape in the form of X-ray fluorescence. This effect is preferable because it makes the IP response curve smoother by compensating for the abrupt increase of the absorption efficiency at the absorption edge.

The image stored in the IP fades with the passage of time after exposure to X-rays. The fading rate depends on the type of IP and the temperature; it increases at higher temperature. But it does not depend on the exposure level or on the X-ray photon energy of the image. Fig. 7.1.8.7 shows the fading of an IP (type BAS III) as a function of time for two different X-ray energies at 293 K. The fading curve can be fitted well with three exponentials:

$$I(t) = A_1 \exp(-k_1 t) + A_2 \exp(-k_2 t) + A_3 \exp(-k_3 t).$$

$1/k_1$, $1/k_2$, and $1/k_3$ are 0.7, 18, and 520 h, respectively.

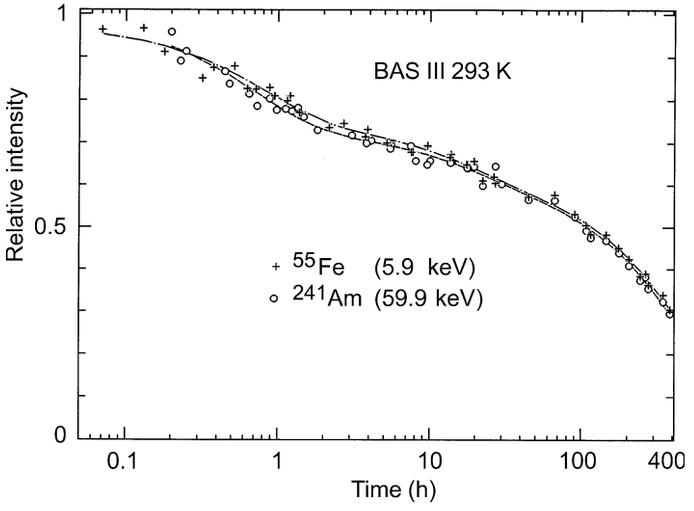


Fig. 7.1.8.7. Fading of the IP signals as a function of time with two different X-ray energies (5.9 and 59.5 keV). Temperature 293 K, type of IP: BAS III (Amemiya, 1995).

The non-uniformity of the response of the IP is about 1–2% over an active area of 250 × 200 mm. The distortion of the image is usually of the order 1%. It depends mainly on the type of IP read-out system.

Since the IP is an integrating-type detector, it is free from instantaneous count-rate limitations, which are accompanied by detectors operating in a pulse-counting mode. Therefore, the IP can make full use of a high flux of synchrotron X-radiation. Using synchrotron X-radiation, time-resolved measurements are possible by mechanically moving the IP (Amemiya, Kishimoto, Matsushita, Satow & Ando, 1989). Caution has been paid not to irradiate extremely intense X-rays (more than $10^6$ photons $\mu m^{-2}$) on the IP; too intense X-rays create either non-erasable colour centres, or colour centres that are seemingly erasable but later reappear.

With minimum precautions, the IP yields reproducible results over a long period of repeated use, unlike X-ray film, whose performance is affected by slight changes in the development conditions. Various kinds of automated IP read-out systems are available, which permit on-site read-out in combination with an X-ray camera. The mechanical flexibility of the IP is also very important when it is used with a Weissenberg camera (Sakabe, 1991).



references